METHODOLOGICAL NOTES

PACS numbers: **44.25.+f**, 47.20.Bp, 47.27.De, 47.55.P–, 92.60.Ox, 92.60.Qx

Rayleigh convective instability in the presence of phase transitions of water vapor. The formation of large-scale eddies and cloud structures

B Ya Shmerlin, M V Kalashnik

DOI: 10.3367/UFNe.0183.201305d.0497

Contents

Abstract. **Convective motions in moist saturated air are accompanied by the release of latent heat of condensation. Taking this effect into account, we consider the problem of convective instability of a moist saturated air layer, generalizing the formulation of the classical Rayleigh problem. An analytic solution demonstrating the fundamental difference between moist convection and Rayleigh convection is obtained. Upon losing stability in the two-dimensional case, localized convective rolls or spatially periodic chains of rollers with localized areas of upward motion evolve. In the case of axial symmetry, the growth of localized convective vortices with circulation characteristic of tropical cyclones (hurricanes) is possible at the early stages of development and on the scale of tornados to tropical cyclones.**

B Ya Shmerlin Typhoon Research and Production Association,
ul. Pobedy 4, 249038 Obninsk, Kaluga region, Russian Federation
Tel. +7 (48439) 7 19 13. Fax +7 (48439) 4 09 10
E-mail: shmerlin@typhoon.obninsk.ru
M V Kalashnik Typhoon Research and Production Association,
ul. Pobedy 4, 249038 Obninsk, Kaluga region, Russian Federation;
Obukhov Institute of Atmospheric Physics, Russian Academy of Sciences,
Pyzhevskii per. 3, 109017 Moscow, Russian Federation
Obninsk Institute for Nuclear Power Engineering
of the National Research Nuclear University MEPhI,
Studgorodok 1, 249040 Obninsk, Kaluga region, Russian Federation
Tel. +7 (48439) 5 23 17. Fax +7 (48439) 4 09 10
E-mail: kalashnik-obn@mail.ru

Received 16 February 2012, revised 30 March 2012
Uspekhi Fizicheskikh Nauk **183** (5) 497 – 510 (2013)
DOI: 10.3367/UFNr.0183.201305d.0497
Translated by S D Danilov; edited by A M Semikhatov

1. Introduction

Convective motions in liquids and gases subject to the field of gravity are generated if their density (temperature) is spatially inhomogeneous. Various forms of convective motion are observed in Earth's atmosphere, which can be considered to be composed of dry air and water vapor. If the water vapor is unsaturated, motions in the atmosphere are described with high accuracy by standard heat convection equations — the Boussinesq equations [1, 2]. The situation changes radically when the vapor is saturated. Because the saturation density decreases with height, the water vapor in rising moist air parcels experiences condensation, accompanied by the release of latent heat of condensation and precipitation. Condensation heating, augmenting the Archimedes buoyancy force, plays an important role in processes of the formation of convective cloudiness in the atmosphere [3–5]. Tropical cyclones or hurricanes — large-scale atmospheric vortices forming over the tropical ocean — furnish one more vivid example of perturbations driven by latent heat release. According to the estimates in Ref. [6] based on the precipitation balance, a condensation heat source in the central part of a hurricane operates at a power of 4×10^8 MW, exceeding that of all US power plants by a factor of 10^3.

A detailed description of moisture phase transition processes is a rather complex problem of cloud microphysics. In studies of the dynamics of moist convection, a simplified approach is typically used based on including a volume latent heat source in the equations of heat convection, which is proportional to the vertical velocity in the ascending branch of circulation, but is absent (zero) in the descending ones. This representation corresponds to the release of latent heat in rising moist air, but to the absence of heat absorption in droplet evaporation in descending air (owing to the absence of droplets). Numerous papers have dealt with generalized statements of the classical Rayleigh problem with the volume latent heat source taken into account, exploring the stability of mechanical equilibrium in a layer of moist saturated air. Because of the nonanalytic (piecewise linear) dependence of the source on the vertical velocity, the analysis was confined to either separate numerical simulations [7–15] or particular solutions for an inviscid atmosphere (lacking thermal conductivity) [16–19]. In this paper, based on the results in Refs [20–23], we propose an analytic solution of the problem, which demonstrates the principal distinctions of moist convection from the Rayleigh convection. The most prominent distinctions are related to the structure of perturbations evolving upon the loss of stability. For instance, in two dimensions, there is a parameter range (for the Rayleigh and Taylor numbers) where localized perturbations corresponding to an isolated convective roll show the fastest growth. For other parameter values, periodic structures related to spatially periodic systems of convective rolls with narrow (concentrated) regions of ascending motion are the most rapidly growing. The intensification of localized axisymmetric structures in a rotating atmosphere illustrates the possibility of spontaneous growth of hurricane vortex perturbations.

The results presented can, in our opinion, be helpful to a broad community of readers interested in particular problems of nonlinear dynamics as well as in general questions about the theory of self-organization (the theory of structure birth) in dissipative media.

2. Conditions for the onset of convection in an ideal (inviscid and lacking thermal conductivity) atmosphere

We begin with known facts related to the stability of an atmospheric column in a homogeneous gravity field. We assume that the thermodynamical parameters p, ρ, and T (pressure, density, and temperature), linked by the equation of state $p = R_{\mathrm{a}}\rho T$, depend only on the vertical coordinate z (directed opposite to the field of gravity) and satisfy the hydrostatic balance equation

$$\frac{\mathrm{d}p}{\mathrm{d}z} = -g\rho\,, \tag{1}$$

where g is the acceleration of gravity and R_{a} is the gas constant. The stability of equilibrium state (1) can be judged by considering adiabatic displacements (without heat exchange) of air parcels between two different levels. As is known [3, 4], the temperature in a rising parcel decreases at the adiabatic lapse rate $\gamma_{\mathrm{a}} = g/c_p$. Here, c_p is the specific heat at constant pressure in dry air and $\gamma_{\mathrm{a}} \approx 1\,\mathrm{K}/100\,\mathrm{m}$. If the condition $\gamma > \gamma_{\mathrm{a}}$ is satisfied, where $\gamma = -\mathrm{d}T/\mathrm{d}z$ is the temperature gradient of ambient air (the convention in meteorology is to take gradients with the negative sign), the parcel is warmer and lighter than its surroundings and continues moving away from its initial position. Such a state is convectively unstable. By contrast, for $\gamma < \gamma_{\mathrm{a}}$, the gravity force returns the colder parcel to its initial position. Hence, in a stable state, the temperature decreases with height more slowly than γ_{a}, i.e., the condition $\gamma < \gamma_{\mathrm{a}}$ must hold. We note that this condition also follows from the general statement that the entropy must increase with height in a stable state [1]. Using Eqn (1) and the explicit expression for the entropy of dry air $\eta = c_p \ln T - (R_{\mathrm{a}}/c_p)\ln p + \mathrm{const}$ [3], we obtain $\mathrm{d}\eta/\mathrm{d}z = c_p T^{-1}(\gamma_{\mathrm{a}} - \gamma) > 0$ for $\gamma < \gamma_{\mathrm{a}}$.

The consideration above pertains to dry air containing unsaturated water vapor. If the water vapor is in a saturated state, the amount of moisture that can be carried by an air parcel decreases with height. As this parcel rises, its water vapor condenses and, because of the latent heat release, the rate at which the parcel temperature decreases with height turns out to be smaller than γ_{a}. The corresponding lapse rate is conventionally called the moist adiabatic lapse rate γ_{m}. From the second law of thermodynamics, it follows for this quantity that [3–5]

$$\gamma_{\mathrm{m}} = \gamma_{\mathrm{a}} + \frac{L_v}{c_p}\frac{\mathrm{d}s_{\mathrm{m}}}{\mathrm{d}z}\,, \tag{2}$$

where L_v is the specific heat of condensation and s_{m} is the mass fraction of saturated vapor (a function of temperature and pressure). When considering convection in the atmosphere, it is commonly assumed that all the condensed moisture precipitates. It then follows that the notion of moist adiabatic lapse rate pertains only to rising air masses. As a parcel moves down, its temperature changes at the dry adiabatic lapse rate γ_{a} (no heat is lost to evaporate droplets).

As regards the gradients γ_{a} and γ_{m}, meteorologists distinguish between the absolutely unstable temperature stratification $\gamma > \gamma_{\mathrm{a}} > \gamma_{\mathrm{m}}$, the moist unstable, but dry stable (conditionally stable) stratification $\gamma_{\mathrm{a}} > \gamma > \gamma_{\mathrm{m}}$, and the moist stable stratification $\gamma_{\mathrm{a}} > \gamma_{\mathrm{m}} > \gamma$. For the conditionally unstable stratification, particles displaced downward return to their initial position, but those displaced upward continue moving away. This principal dependence on the direction of vertical displacement is one of the main distinctive features of the dynamics of convective processes in moist saturated air.

3. Statement of the problem of convective instability in a layer of moist saturated air

In Section 2, we neglected the dissipative factors (viscosity and thermal conductivity). Here, we consider the statement of the problem of the stability of mechanical equilibrium, similar to the statement of the classical Rayleigh problem [1, 2]. There is a layer of rotating viscous and heat conducting atmosphere of thickness h, saturated with water vapor and bounded by two rigid horizontal surfaces. The surfaces are kept at constant temperatures, and hence the temperature distribution at equilibrium is a linear function of the vertical coordinate. We need to explore the stability of the equilibrium state, with the release of latent heat of condensation in ascending motions of saturated air taken into account.

We analyze stability in the framework of the system of equations that is traditionally used to numerically simulate atmospheric convection [24, 25]. In this system, the molecular coefficients of viscosity and thermal conductivity are replaced by their turbulent analogs (which model the effect of small-scale stochastic convection). Additionally, we assume that the turbulent exchange is anisotropic, differing in the horizontal and vertical directions. With these assumptions, the behavior of small perturbations of the equilibrium state obeys the system of equations

$$\begin{aligned} &\mathbf{u}_t + f\mathbf{k}\times\mathbf{u} = -\nabla p + g\theta\mathbf{k} + \mu\Delta\mathbf{u} + \nu\mathbf{u}_{zz}\,, \qquad \operatorname{div}\mathbf{u} = 0\,, \\ &\theta_t + \Gamma w = \mu\Delta\theta + \nu\theta_{zz} + Q\,, \end{aligned} \tag{3}$$

which is to be augmented with the Rayleigh boundary conditions (the slip conditions) on the horizontal boundaries,

$$u_z = v_z = w = \theta = 0\,, \qquad z = 0, h\,. \tag{4}$$

Here, $\mathbf{u}$ is the velocity vector with the respective components u, v, and w along the horizontal x and y axes and the vertically directed z axis, $p = p'/\bar{\rho}$, $\theta = \alpha T'$, where p' and T' are the deviations of pressure and temperature from their equilibrium distributions, α is the thermal expansion coefficient, $\bar{\rho}$ is a constant reference density, $\Gamma = \alpha(\gamma_a - \gamma)$ is the stratification parameter, $\gamma = -\mathrm{d}\bar{T}/\mathrm{d}z$ is the temperature gradient in the equilibrium, μ and v are the turbulent exchange coefficients in the horizontal and vertical directions, f is the Coriolis parameter, Δ is the two-dimensional (horizontal) Laplace operator, $\mathbf{k}$ is a unit vertical vector, and $Q = \alpha M/c_p$, M [W kg^{-1}] is the heat source intensity. Letter subscripts are used here and below to denote partial derivatives.

The source related to the release of latent condensation heat is represented as $M = -L_v w(\mathrm{d}s_m/\mathrm{d}z)$ for the ascending saturated air and $M = 0$ for the descending flow [7–19]. In terms of the Heaviside function [$H(w) = 1, w > 0$; $H(w) = 0, w < 0$], the source can be written as

$$M = c_p(\gamma_a - \gamma_m)wH(w)\,, \tag{5}$$

where the moist adiabatic gradient γ_m is given by expression (2). As mentioned above, representation (5) implies that water vapor condensation occurs in ascending air masses, while all the condensate precipitates as rain. The moist adiabatic gradient depends in general on the temperature and pressure of the equilibrium state. This dependence is neglected in this paper, and γ_m is treated as constant.

We note that the continuity equation is written in system (3) for an incompressible fluid. The approximation of incompressibility is valid for describing convection in shallow atmospheric layers. Its applicability conditions are given, e.g., in Ref. [24].

System (3) with source (5) belongs to the class of systems with nonanalytic (piecewise-linear or 'jumping') nonlinearities. This nonlinearity does not allow linearization, even in principle. The presence of a nonlinear source is a distinctive mathematical feature of this problem.

We seek a solution of problem (3)–(5) in the quasistatic approximation. In this approximation, the vertical projection of the momentum equation reduces to the hydrostatic balance $p_z = g\theta$. The quasistatic variant of system (3) with boundary conditions (4) allows a separation of variables: both the solution and the source can be expanded in series in eigenfunctions $\cos(\pi nz/h)$ and $\sin(\pi nz/h)$ of the operator $\mathrm{d}^2/\mathrm{d}z^2$. We consider the case $n = 1$ (the first vertical mode) and assume that

$$(u, v, p) = (\tilde{u}, \tilde{v}, \tilde{p}) \cos\frac{\pi z}{h}\,, \qquad (w, \theta, Q) = (\tilde{w}, \tilde{\theta}, \tilde{Q}) \sin\frac{\pi z}{h}\,,$$

where the parentheses combine amplitudes that are independent of z. Eliminating the pressure using the hydrostatic equation, we arrive at a system of three equations for $\tilde{w}$, $\tilde{\theta}$ and the vertical component of vorticity $\tilde{\omega} = \tilde{v}_x - \tilde{u}_y$. As scales for the variables t, x, y, $\tilde{w}$, and $\tilde{\omega}$, we select d^2/v, $\sqrt{\mu/v}\,d$, $\sqrt{\mu/v}\,d$, gd^2/μ, and $vg/(\mu f d)$, where $d = h/\pi$. Suppressing the tilde in what follows, we write the system of equations for the dimensionless amplitudes:

$$\begin{aligned} &w_t - \Delta w + w + \omega + \Delta\theta = 0\,, \qquad \omega_t - \Delta\omega + \omega - Tw = 0\,, \\ &\theta_t - \Delta\theta + \theta + Rw = Q\,, \qquad Q = R_m wH(w)\,, \end{aligned} \tag{6}$$

which contains three dimensionless parameters

$$R = \frac{\alpha g(\gamma_a - \gamma)d^4}{\mu v}\,, \qquad T = \frac{f^2 d^4}{v^2}\,, \qquad R_m = \frac{\alpha g(\gamma_a - \gamma_m)d^4}{\mu v}\,. \tag{7}$$

Here, R_m is the parameter characterizing the intensity of latent heat release and R is an analog of the Rayleigh number. In expression (7) and below, T is an analog of the Taylor number. We note that the form of the Rayleigh number used here differs from the traditional one [1, 2] by its sign and the factor π^4 in the denominator. The Ekman number $E = 1/\sqrt{T}$ can often be conveniently used instead of the Taylor number. The goal of the subsequent analysis lies in determining the critical values of the parameters R and T marking the boundary for the emergence of unstable solutions of system (6) when the external parameter R_m is fixed, and in exploring their structure.

We note that the quasistatic approximation does not interfere with the main mathematical aspect of the problem related to the source nonlinearity. This approximation is also frequently adopted in atmospheric numerical models; it is valid under conditions of strong anisotropic exchange $\mu \gg v$.

4. Critical values for 'dry' convection

We begin by seeking critical values of parameters in dry convection. For $R_m = 0$, system (6) reduces to the single equation

$$(\partial_t - \Delta + 1)^2 w + Tw - R\Delta w = 0\,. \tag{8}$$

Seeking exponentially increasing solutions of Eqn (8) in the form $w = \exp(\kappa t)\exp[\mathrm{i}(k_1 x + k_2 y)]$, we find the growth increment

$$\kappa_{1,2} = -(k^2 + 1) \pm \sqrt{-Rk^2 - T}\,, \qquad k^2 = k_1^2 + k_2^2\,.$$

Setting $\kappa_1 = 0$, we find the critical value for the Rayleigh number associated with a given value of the wave vector modulus k: $R = R_{cr}(k, T) = -((1 + k^2)^2 + T)/k^2$. Perturbations grow for $R < R_{cr}(k, T)$ and decay for $R > R_{cr}(k, T)$. A physical meaning is given to the maximum value $R = R_{cr}(k, T)$ attained at some $k = k_{cr}(T)$ and related to the most dangerous perturbation

$$R = R_{cr}(T) = -2\left(\sqrt{1 + T} + 1\right)\,, \qquad k_{cr}^2 = \sqrt{1 + T}\,. \tag{9}$$

The curve $R = R_{cr}(T)$ in the parameter plane $(T^{1/2}, R)$ separates regions of stability and instability (Fig. 1). Values $T^{1/2} < 0$ are associated with $f < 0$. The most dangerous perturbation is given by a system of convective cells with the horizontal size $S = \pi/k_{cr}$.

For comparison, we present the critical values obtained without the quasistatic approximation. It can be easily shown that in the absence of background rotation, the full system (3) (with the same normalization) leads to $R_{cr}(k, T) = -(1 + k^2)^2(1 + \varepsilon k^2)/k^2$, where $\varepsilon = v/\mu$. For the most rapidly growing perturbation and isotropic exchange $\varepsilon = 1$, we recover the classical result of Rayleigh [1, 2]: $R_{cr} = -27/4$

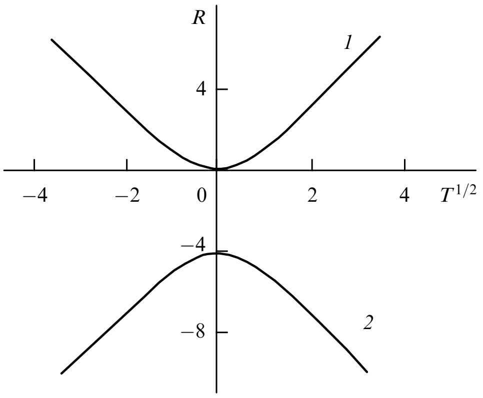

Figure 1. *1* — the curve $R = R_1(0, T)$ separating domains with different structures of the Green's function. *2* — the curve $R = R_{cr}(T)$ in the parameter plane $(\sqrt{T} \equiv E^{-1}, R)$; the instability domain of the dry Rayleigh convection is below the curve.

and $k_{cr} = \sqrt{2}/2$. The respective values (9) in the quasistatic approximation become $R_{cr} = -4$ and $k_{cr} = 1$, i.e., differ by a factor of more than one and a half. However, if the exchange is anisotropic, $\varepsilon \ll 1$, we obtain $R_{cr} \approx -4(1 + 2\varepsilon)$ and $k_{cr} \approx 1 - \varepsilon$ and, accordingly, the quasistatic approximation then leads to asymptotically exact results.

5. Green's function. Integral equation for the vertical velocity amplitude

We can try to construct solutions of nonlinear system (6) separately in dry ($w < 0$) and moist ($w > 0$) regions, and then match them at the boundary of the regions. Such an approach results in cumbersome computations. More efficient is the approach comprising two stages, as proposed in Refs [20–23]. At the first stage, the Green's function for the problem with a given heat source is constructed. Then, in the formula for the vertical velocity, which represents the convolution of the heat source with the Green's function, the heat source Q is substituted in form (6), which yields an integral equation for the vertical velocity amplitude. The analysis of this integral equation allows finding both the structure and the increment of unstable perturbations dependent on the problem parameters.

To construct the Green's function, it is convenient to rewrite system (6) in the vector–matrix form [26]

$$\mathbf{q}_t + A\Delta\mathbf{q} + B\mathbf{q} = \mathbf{F}\,,$$
$$A = \begin{pmatrix} -1 & 0 & 1 \\ 0 & -1 & 0 \\ 0 & 0 & -1 \end{pmatrix}, \qquad B = \begin{pmatrix} 1 & 1 & 0 \\ -T & 1 & 0 \\ R & 0 & 1 \end{pmatrix}, \tag{10}$$

where $\mathbf{q} = (w, \omega, \theta)^{\mathrm{tr}}$ and $\mathbf{F} = (0, 0, Q)^{\mathrm{tr}}$ (the superscript here denotes transposition). Seeking exponentially increasing solutions $\mathbf{q} = \exp(\kappa t)\,\mathbf{q}(x, y)$ and $\mathbf{F} = \exp(\kappa t)\,\mathbf{F}(x, y)$, we reduce Eqn (10) to the stationary equation

$$\Delta\mathbf{q} - C\mathbf{q} = A^{-1}\mathbf{F}\,, \qquad C = -A^{-1}(B + \kappa I)\,, \tag{11}$$

where I is the identity matrix. The eigenvalues λ_j^2 of the matrix C are different,

$$\lambda_{1,2}^2 = 1 + \kappa + \frac{R}{2} \pm \sqrt{\frac{R^2}{4} + R(1+\kappa) - T}\,, \qquad \lambda_3^2 = 1 + \kappa\,, \tag{12}$$

and therefore a matrix U exists that diagonalizes C. Inserting $\mathbf{q} = U\boldsymbol{\sigma}$ into Eqn (11) and multiplying by U^{-1}, we obtain the system of three Helmholtz equations $\Delta\sigma_j - \lambda_j^2\sigma_j = \tilde{F}_j$, where the right-hand sides $\tilde{F}_j$ are linear functions of the heat source Q. Solutions of these equations are convolutions of $\tilde{F}_j$ with the well-known Green's functions of the Helmholtz equation. Performing the inverse linear transformation, for each of the components w, ω, and θ of the vector $\mathbf{q}$, we obtain expressions that are convolutions of the heat source with the corresponding Green's functions, which are linear combinations of the Green's functions of the Helmholtz equation. The substitution of the source $Q = R_{\mathrm{m}} w H(w)$ in the expression for w results in the sought integral equation for the vertical velocity amplitude. If w depends only on the coordinate x (the planar geometry of the problem), the equation takes the form

$$w(x) = R_{\mathrm{m}} \int_{w>0} G(x - x')\, w(x')\, \mathrm{d}x'\,, \tag{13}$$

$$G(x) = \frac{1}{\lambda_1^2 - \lambda_2^2}\Big(\lambda_1 \exp\left(-\lambda_1|x|\right) - \lambda_2 \exp\left(-\lambda_2|x|\right)\Big)\,. \tag{14}$$

In general, we have the equation

$$w(x, y) = R_{\mathrm{m}} \iint_{w>0} G(x - x', y - y')\, w(x', y')\, \mathrm{d}x'\, \mathrm{d}y'\,, \tag{15}$$

$$G(x, y) = \frac{1}{2\pi(\lambda_1^2 - \lambda_2^2)}\left(\lambda_1^2 K_0(\lambda_1 r) - \lambda_2^2 K_0(\lambda_2 r)\right)\,, \qquad r = \sqrt{x^2 + y^2}\,, \tag{16}$$

where $K_0(r)$ is the cylindrical Macdonald function. We stress that the integration in Eqns (13) and (15) ranges the regions $w > 0$, which are a priori unknown and have to be found in the solution process.

We detail the structure of the Green's function for vertical velocity (14), which is dependent on the eigenvalues $\lambda_{1,2}^2$. We set

$$R_{1,2}(\kappa, T) = \pm 2\Big(\sqrt{1 + \kappa^2 + T} \mp (1 + \kappa)\Big)\,.$$

It follows from Eqn (12) that the eigenvalues $\lambda_{1,2}^2$ are positive for $R > R_1(\kappa, T)$, negative for $R < R_2(\kappa, T)$, and complex-conjugate for $R_2 < R < R_1$. In the case of positive eigenvalues $\lambda_{1,2}^2$, the Green's function is localized in the vicinity of the heat source, $G(0) = 1/(\lambda_1 + \lambda_2) > 0$. On the semiaxis $x > 0$, it changes sign only once, passing through the point $x_G = (\lambda_1 - \lambda_2)^{-1} \ln(\lambda_1/\lambda_2)$, and monotonically decays at infinity. The complex-conjugate values $\lambda_{1,2}^2$ are written as $\lambda_{1,2} = \xi_2 \pm \mathrm{i}\xi_1$, where $\xi_2 = 0.5\sqrt{R - R_2}$ and $\xi_1 = 0.5\sqrt{R_1 - R}$. The corresponding Green's function

$$G(x) = \delta \exp\left(-\xi_2|x|\right) \cos\left(\xi_1|x| + \chi\right)\,,$$

with $\delta = (\xi_1^2 + \xi_2^2)^{1/2}/(4\xi_1\xi_2)$ and $\tan\chi = \xi_2/\xi_1$, manifests oscillations and changes its sign infinitely many times. The curve $R = R_1(0, T)$ separating the domains with different Green's function behaviors is shown in Fig. 1. The curve $R = R_2(0, T)$ coincides with the critical curve (9) for the Rayleigh convection (curve *2* in Fig. 1). As this curve is approached, $G(x) \to \infty$ and the spatial period of the Green's function oscillations $2\pi/\xi_1$ tends to that of the most dangerous perturbations for the dry Rayleigh convection, Eqn (9), while spatial decay disappears. As the Rayleigh number approaches the boundary $R = R_1(0, T)$ dividing the regions with different behaviors of the Green's function, the spatial period of the Green's function oscillations tends to infinity, and the boundary is traversed in a continuous way.

By its physics, the Green's function for the components w, ω, and θ describes the circulation created by a point-like horizontal heat source. Because ascending motions are accompanied by latent heat release, it is apparent on the physical level that the structure of most unstable perturbations in a moist atmosphere must derive from the spatial structure of the Green's function for the vertical velocity. In the case of localized Green's function and for the heat release (the value of R_m) sufficiently large, most rapidly growing perturbations are localized. If the Green's function oscillates, the most rapid growth is experienced by spatially periodic structures, whose period of spatial oscillations is determined by that of the Green's function. The analysis in what follows substantiates these assumptions with rigorous mathematical results.

In Section 6, we construct localized and periodic solutions of Eqn (13). In constructing periodic solutions with a period $2L_*$, Green's function (14) is replaced, for convenience, by the periodic Green's function

$$G_{L_*}(x) = \frac{1}{2(\lambda_1^2 - \lambda_2^2)} \times \left(\frac{\lambda_1 \cosh\big(\lambda_1 (L_* - |x|)\big)}{\sinh(\lambda_1 L_*)} - \frac{\lambda_2 \cosh\big(\lambda_2 (L_* - |x|)\big)}{\sinh(\lambda_2 L_*)} \right). \quad (17)$$

This function is a linear combination of the Green's functions for boundary value problems with the periodicity conditions $\sigma_j'' - \lambda_j^2 \sigma_j = \tilde{F}_j$, $\sigma_j(-L_*) = \sigma_j(L_*)$, and $\sigma_j'(-L_*) = \sigma_j'(L_*)$. Green's function (14) is the limit of (17) as $L_* \to \infty$.

6. Convective instability under two-dimensional planar perturbations. Periodic and localized structures

6.1 Periodic solutions

We seek periodic solutions (with the period $2L_*$) of Eqn (13) with kernel (17) in the class of even functions satisfying conditions of sign-definiteness $w \geqslant 0$, $x \in (0, x_0)$; $w \leqslant 0$, $x \in (x_0, L_*)$. To find $w(x)$ in the moist domain $x \in (0, x_0)$, we use Eqn (13) to obtain the equation

$$w(x) = R_m \int_0^{x_0} \big(G_{L_*}(x - x') + G_{L_*}(x + x') \big)\, w(x')\, dx', \quad (18)$$

with the obvious boundary condition $w(x_0) = 0$. After the solution in the moist region is found, the expression for $w(x)$ in the dry region $x \in (x_0, L_*)$ is obtained by integration in Eqn (18). Equation (18) differs from the classical Fredholm equation because its solution is subject to a rather strong constraint of sign definiteness and the parameter x_0 (the radius of the precipitation region) has to be determined in the course of solving.

In the region $x \in (0, x_0)$, system (6) can be reduced to a single fourth-order linear differential equation for $w(x)$. Because the solution of Eqn (18) belongs to the class of even functions, we seek it (up to a factor) in the form

$$w(x) = \frac{\cos(p_1 x)}{\cos(p_1 x_0)} - \frac{\cos(p_2 x)}{\cos(p_2 x_0)}, \qquad 0 < x < x_0, \quad (19)$$

with real-valued coefficients p_1 and p_2 undefined at this stage. The boundary condition is automatically satisfied in this case. The substitution of Eqn (19) in Eqn (18) leads to terms proportional to $\cos(p_j x)$ and $\cosh(\lambda_j x)$ in the right-hand side. Equating the coefficients with $\cos(p_j x)$ in the left- and right-hand sides, we obtain the equation for p_j,

$$p_j^4 + (\lambda_1^2 + \lambda_2^2 - R_m)\, p_j^2 + \lambda_1^2 \lambda_2^2 = 0, \qquad j = 1, 2.$$

Assuming, for definiteness, that $p_2 > p_1$, we find

$$p_{1,2} = 0.5\sqrt{R_m}\big(\sqrt{1-\lambda} \mp \sqrt{1-\lambda_0}\,\big), \quad \lambda = \frac{(\lambda_1 - \lambda_2)^2}{R_m}, \quad \lambda_0 = \frac{(\lambda_1 + \lambda_2)^2}{R_m}; \quad \lambda_{1,2} = 0.5\sqrt{R_m}\big(\sqrt{\lambda_0} \pm \sqrt{\lambda}\,\big). \quad (20)$$

In the plane of parameters λ_0 and λ, which play an important role in what follows, the real values of $p_2 > p_1$ are associated with the region $\lambda \leqslant \lambda_0 \leqslant 1$. The quantities $\lambda_{1,2}$ are real-valued in the region $0 \leqslant \lambda \leqslant \lambda_0 \leqslant 1$ and are complex conjugate for $0 \leqslant \lambda_0 \leqslant 1$, $\lambda < 0$.

Equating the coefficient with $\cosh(\lambda_j x)$ in Eqn (18) to zero, we obtain the equations

$$\frac{p_2 \tan(p_2 x_0) - \lambda_j \tanh(\lambda_j L)}{p_2^2 + \lambda_j^2} - \frac{p_1 \tan(p_1 x_0) - \lambda_j \tanh(\lambda_j L)}{p_1^2 + \lambda_j^2} = 0, \qquad j = 1, 2,$$

where $L = L_* - x_0$. They can be conveniently solved for $\tan(p_{1,2} x_0)$:

$$\tan(p_1 x_0) = 0.5(B_1 - B_2), \quad \tan(p_2 x_0) = -0.5(B_1 + B_2). \quad (21)$$

Taking the last relations in (20) into account, for $\lambda \geqslant 0$, we have

$$B_1 = \sqrt{\lambda_0^{-1} - 1}\,\Big(\tanh\big((\sqrt{\lambda} + \sqrt{\lambda_0})Z\big) + \tanh\big((\sqrt{\lambda_0} - \sqrt{\lambda})Z\big)\Big), \quad B_2 = \sqrt{\lambda^{-1} - 1}\,\Big(\tanh\big((\sqrt{\lambda} + \sqrt{\lambda_0})Z\big) - \tanh\big((\sqrt{\lambda_0} - \sqrt{\lambda})Z\big)\Big), \quad Z = 0.5\sqrt{R_m}\, L. \quad (22)$$

For $\lambda < 0$, passing from hyperbolic to trigonometric functions, we obtain

$$B_1 = D^{-1}\sqrt{\lambda_0^{-1} - 1}\, \sinh\big(2\sqrt{\lambda_0}\, Z\big), \quad B_2 = D^{-1}\sqrt{1 + |\lambda|^{-1}}\, \sin\big(2\sqrt{|\lambda|}\, Z\big), \quad D = \cos^2\big(\sqrt{|\lambda|}\, Z\big) + \sinh^2\big(\sqrt{\lambda_0}\, Z\big). \quad (23)$$

Further analysis reduces, in fact, to finding the solvability conditions for Eqns (21) and verifying that the sign-definiteness condition holds for their solutions. As follows from the analysis, for complex-valued p_1 and p_2, Eqns (21) are necessarily incompatible [this, in particular, was the rationale for form (19)].

Equations (21) lead to the relations

$$p_1 x_0 = \arctan\big(0.5(B_1 - B_2)\big) + \pi n, \quad p_2 x_0 = -\arctan\big(0.5(B_1 + B_2)\big) + \pi m, \quad (24)$$

where n and m are some natural numbers. Because $B_1 > 0$ and $p_2 > p_1$, it should certainly be $m > n$. In what follows, we refer to the solutions that correspond to different n and m as the modes. Taking Eqns (20) into account and adding Eqns (24), we arrive at

$$x_0 = \frac{1}{\sqrt{R_m(1-\lambda)}}\Big((n+m)\pi + \arctan\big(0.5(B_1 - B_2)\big) - \arctan\big(0.5(B_1+B_2)\big)\Big)\,. \tag{25}$$

Eliminating the parameter x_0 from Eqn (25), we obtain the equation

$$F(\lambda_0, \lambda, Z) \equiv \pi m - \arctan\big(0.5(B_1+B_2)\big) - \frac{\sqrt{1-\lambda}+\sqrt{1-\lambda_0}}{\sqrt{1-\lambda}-\sqrt{1-\lambda_0}}\Big(\pi n + \arctan\big(0.5(B_1-B_2)\big)\Big) = 0\,, \tag{26}$$

which defines a functional dependence between the parameters λ_0, λ, and Z and ensures the existence of nontrivial periodic solutions of integral equation (18). For each mode in the parameter plane (λ_0, λ), dependence (26) defines a one-parametric curve family $\lambda = f(\lambda_0, Z)$ (with the parameter Z) such that a solution exists at each point on the curves. For a fixed Z, the curve corresponds to a periodic solution with $L = 2Z/\sqrt{R_m}$ and the value of x_0 given by expression (25).

6.2 Localized solutions

The localized solutions can be obtained similarly by replacing the periodic Green's function G_{L_*} in Eqn (18) with the Green's function G for a point-like heat source, Eqn (14). On the other hand, localized solutions can be treated as periodic ones with an infinite period, which is realized at $Z = \infty$. If $Z = \infty$, it follows from Eqns (22) and (23) that $B_1 = (\lambda_0^{-1} - 1)^{1/2}$ and $B_2 = 0$, and Eqns (21) reduce to

$$\tan(p_1 x_0) = \sqrt{\lambda_0^{-1} - 1}\,, \qquad \tan(p_2 x_0) = -\sqrt{\lambda_0^{-1} - 1}\,.$$

Hence, instead of (24)–(26), we have

$$p_1 x_0 = \arctan\sqrt{\lambda_0^{-1} - 1} + \pi n\,, \qquad p_2 x_0 = -\arctan\sqrt{\lambda_0^{-1} - 1} + \pi m\,, \tag{27}$$

$$x_0 = \frac{\pi(n+m)}{\sqrt{R_m(1-\lambda)}}\,, \tag{28}$$

$$\lambda = f(\lambda_0) = 1 - (1-\lambda_0)\times\left(\frac{m-n}{m+n} - \frac{2}{\pi(m+n)}\arcsin\sqrt{1-\lambda_0}\right)^{-2}. \tag{29}$$

Dependence (29) ensures the existence of localized solutions of Eqn (18). The parameters n and m are selected so as to satisfy the condition of sign definiteness.

6.3 Mode existence regions in the plane (λ_0, λ)

Finding these regions allows determining the instability domain in the plane of initial problem parameters. A detailed analysis of the behavior of curves $\lambda = f(\lambda_0, Z)$ for different modes is performed in Refs [20–23]. For each mode in the region $0 \leqslant \lambda \leqslant \lambda_0 \leqslant 1$, which corresponds to real-valued $\lambda_{1,2}$, the curves $\lambda = f(\lambda_0, Z)$ drawn for different Z do not intersect and are located to the left of the curve $\lambda = f(\lambda_0)$ for the localized mode $Z = \infty$. Figure 2 plots these curves for the mode $n = 0$, $m = 1$. In the domain $\lambda < 0$ that corresponds to the complex-conjugate $\lambda_{1,2}$, the curves $\lambda = f(\lambda_0, Z)$ for different Z multiply intersect each other. For a fixed Z, the

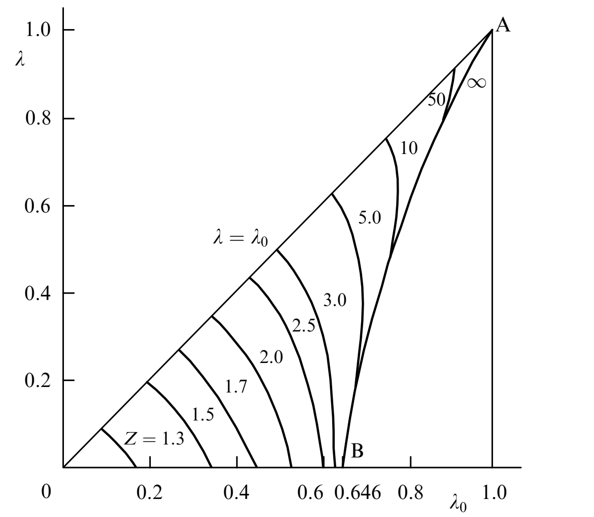

Figure 2. Curves $\lambda = f(\lambda_0, Z)$ for various Z in the region $0 \leqslant \lambda \leqslant \lambda_0 \leqslant 1$ for the mode $n = 0$, $m = 1$. AB is the curve $\lambda = f(\lambda_0)$ for the localized mode $n = 0$, $m = 1$.

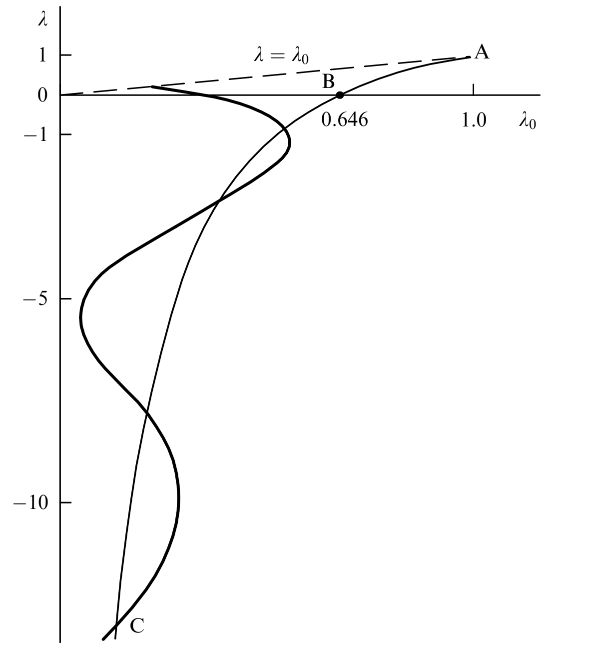

Figure 3. Curve $\lambda = f(\lambda_0, Z)$ for $Z = 1.5$ for the mode $n = 0$, $m = 1$ (thick solid line); ABC is the curve $\lambda = f(\lambda_0)$ for the localized mode $n = 0$, $m = 1$.

curve $\lambda = f(\lambda_0, Z)$ winds around the curve $\lambda = f(\lambda_0)$, as shown in Fig. 3 for the mode $n = 0$, $m = 1$. We call the intervals of the curve $\lambda = f(\lambda_0, Z)$ lying to the right of $\lambda = f(\lambda_0)$ crests, and those to the left, troughs. For every curve, we enumerate the crests and troughs in the order from top down. Crests and troughs with a fixed number form one-parametric families with Z as a parameter. We find envelopes of these families in the plane (λ_0, λ). The equations for envelopes are obtained by eliminating the parameter Z from the systems of equations $F(\lambda_0, \lambda, Z) = 0$ and $F_Z(\lambda_0, \lambda, Z) = 0$. Using Eqns (26) and (23), it can be readily shown that $F_Z(\lambda_0, \lambda, Z) = 0$ for

$$Z = \frac{\pi j}{2\sqrt{|\lambda|}}\,, \qquad j = 1, 2, \ldots\,. \tag{30}$$

It follows from Eqn (23) that $B_2 = 0$ on the envelopes. Substituting the values Z found above in Eqns (23) and (26)

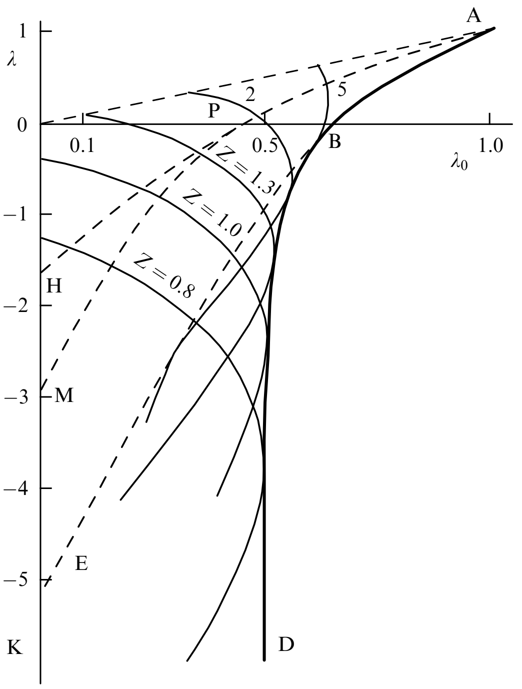

Figure 4. The domain in the plane (λ_0, λ) where the problem solutions exist. The boundary of domain ABD is the curve $\lambda = \psi(\lambda_0)$.

results in equations for the envelopes

$$\arctan\left(\sqrt{\lambda_0^{-1}-1}\,\tanh^{(-1)^j}\left(\frac{j\pi\sqrt{\lambda_0}}{2\sqrt{|\lambda|}}\right)\right) = \frac{\pi}{2}\left((m-n)-(n+m)\sqrt{\frac{1-\lambda_0}{1+|\lambda|}}\right). \qquad (31)$$

It can be easily verified that the envelopes are smooth continuations of curves $\lambda = f(\lambda_0)$ for the corresponding localized modes into the region $\lambda < 0$. In Eqns (30) and (31), $j = 1$ pertains to the envelope of the first crests, $j = 2$ to that of the second troughs, etc. For each mode, the envelope of the first crests $j = 1$ lies to the right of all other envelopes in the plane (λ_0, λ). For the mode $n = 0$, $m = 1$, it has the asymptotic form

$$\lambda_0 = \frac{1}{2}, \qquad \lambda \to -\infty. \qquad (32)$$

Figure 4 shows the envelope BD of the family of the first crests ($j = 1$) and the envelope BE of the family of the second troughs ($j = 2$, the dashed curve); it also plots several curves $\lambda = f(\lambda_0, Z)$ for the mode $n = 0$, $m = 1$ for illustration. The curve AB is $\lambda = f(\lambda_0)$ for this mode in the region $\lambda > 0$. Among the dashed curves, PM is the envelope of the first crests ($j = 1$), PH the envelope of second troughs ($j = 2$), and AP is the curve $\lambda = f(\lambda_0)$ for the mode $n = 0$, $m = 2$ in the region $\lambda > 0$.

Relation (30) implies that the envelope is touched at the point λ by the curve $\lambda = f(\lambda_0, Z)$, with the parameter Z in (30). Thus, each point λ of the envelope is associated with the solution for which

$$L = \frac{j\pi}{\sqrt{R_{\mathrm{m}}|\lambda|}}, \quad \frac{x_0}{L} = \frac{n+m}{j\sqrt{1+|\lambda|^{-1}}}, \quad x_0 = \frac{(n+m)\pi}{\sqrt{R_{\mathrm{m}}\left(1+|\lambda|\right)}}. \qquad (33)$$

6.4 Sign-definiteness and spatial structure of modes

We analyze the structure of localized solutions and the solutions that correspond to envelopes, for different modes. Because $B_2 = 0$, it follows from Eqns (24) and (27) that $\cos(p_2 x_0) = (-1)^{m-n}\cos(p_1 x_0)$. Thus, in the region $x \in (0, x_0)$, up to a positive factor, $w(x) = (-1)^n[\cos(p_1 x) + (-1)^{m-n+1}\cos(p_2 x)]$. Using this relation, together with Eqns (24) and (27), it can be readily shown that the condition of sign definiteness in the moist domain $w \geqslant 0$, $x \in (0, x_0)$ is only satisfied for modes $n = 0$, $m = 1$ and $n = 0$, $m = 2$. Solutions that correspond to these two cases are respectively referred to as the first and the second mode. The localized first and second modes are sign definite in the dry region $x_0 < x < \infty$ for $\lambda \geqslant 0$ on the respective curves $\lambda = f(\lambda_0)$ and sign indefinite for $\lambda < 0$. This follows from the fact that the Green's function G is oscillating for $\lambda < 0$. The periodic first and second modes are sign definite in the dry domain $x_0 \leqslant x \leqslant L_*$ only on the envelopes of first crests ($j = 1$) and second troughs ($j = 2$) of these modes. For these modes on the curves $\lambda = f(\lambda_0, Z)$ at a fixed Z, the solution becomes sign indefinite (in the dry region) immediately after the curve touches the envelope of the second troughs. For modes $n > 0$, $w(x)$ fails to satisfy the condition of sign definiteness not only on the envelopes but also everywhere on the curves $\lambda = f(\lambda_0, Z)$.

Hence, the existence domain for the problem solutions coincides with the corresponding domain for the first mode. On the plane (λ_0, λ), the boundary of the solution existence domain is curve AD in Fig. 4. It consist of two curves smoothly matching each other at $\lambda = 0$: the curve $\lambda = f(\lambda_0)$, Eqn (29), for the first localized mode $n = 0$, $m = 1$ in the region $\lambda \geqslant 0$ and envelope (31) of the first crests $j = 1$ of this mode in the region $\lambda < 0$. Curve AD is denoted as $\lambda = \psi(\lambda_0)$ in what follows. At each point on the curve $\lambda = \psi(\lambda_0)$, the spatial structure of both localized and periodic solutions in the moist domain is given by Eqn (19), which can be conveniently rewritten as

$$w(x) = \cos\left(\frac{\pi}{2}\frac{x}{x_0}\right)\cos\left(\frac{\pi}{2}\sqrt{\frac{1-\lambda_0}{1-\lambda}}\frac{x}{x_0}\right), \quad 0 \leqslant x \leqslant x_0. \quad (34)$$

For localized solutions in the dry domain, after integration in Eqn (18), we have

$$w(x) = -\sqrt{\frac{(1-\lambda)(1-\lambda_0)}{\lambda}}\sinh\left(\frac{\pi}{2}\sqrt{\frac{\lambda}{1-\lambda}}\frac{x-x_0}{x_0}\right) \times \exp\left(-\frac{\pi}{2}\sqrt{\frac{\lambda_0}{1-\lambda}}\frac{x-x_0}{x_0}\right), \quad x > x_0. \qquad (35)$$

For periodic solutions, which correspond to the envelope, we similarly obtain

$$w(x) = -\Lambda\cosh\left(\frac{\pi}{2}\sqrt{\frac{\lambda_0}{|\lambda|}}\left(1-\frac{x-x_0}{L}\right)\right)\sin\left(\frac{\pi}{2}\frac{x-x_0}{L}\right), \quad x_0 < x \leqslant L_*, \qquad (36)$$

$$\Lambda = \sqrt{\frac{(1-\lambda)(1-\lambda_0)}{|\lambda|\lambda_0}}\sin\left(\frac{\pi}{2}\sqrt{\frac{1-\lambda_0}{1-\lambda}}\right)\sinh^{-1}\left(\frac{\pi}{2}\sqrt{\frac{\lambda_0}{|\lambda|}}\right).$$

In relations (34)–(36), x_0 and L are defined by expressions (28) and (33), and λ and λ_0 are linked by the equation $\lambda = \psi(\lambda_0)$. On passing through the point $\lambda = 0$, the spatial structure of the solution that corresponds to the domain boundary $\lambda = \psi(\lambda_0)$ varies continuously. The existence boundary for

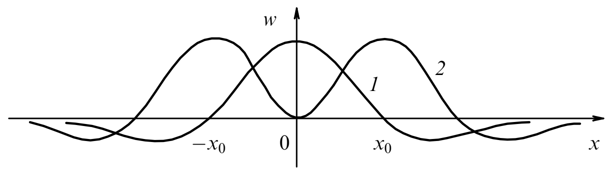

Figure 5. Spatial distributions of the vertical velocity $w(x)$ for the first (*1*) and second (*2*) localized modes.

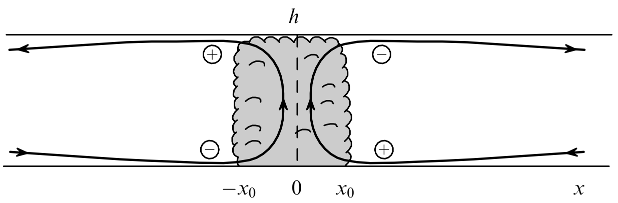

Figure 6. Schematic for the streamlines of the first localized mode in the xz plane. The plus sign corresponds to the velocity component v directed from the reader, and the minus, toward the reader.

the second mode $n = 0$, $m = 2$ is organized similarly and is located in the plane (λ_0, λ) to the left of the curve $\lambda = \psi(\lambda_0)$. The existence domains for periodic sign-definite modes $n = 0$, $m > 2$ are located even further to the left (for these modes, sign-definite localized solutions and sign-definite solutions corresponding to envelopes do not exist).

Given the distributions $w(x)$, we can uniquely find the velocity components u and v by noting that the vortex component v arises in this case owing to the Coriolis force. Plots of the $w(x)$ distributions for the first and second localized modes are shown in Fig. 5. A schematic of streamlines in the xz plane, corresponding to the first mode, is presented in Fig. 6. The modes found describe localized convective rolls exponentially growing with time. The structure of circulation in the convective rolls corresponds to the air inflow onto the symmetry axis in the lower half of the layer and outflow in the upper one. The rise of air in the vicinity of the axis is accompanied by condensation and precipitation. The circulation is respectively cyclonic or anticyclonic in the lower or upper half of the layer.

Figure 7 plots $w(x)$ profiles that correspond to envelopes of the first crests and second troughs for modes $n = 0, m = 1$ and $n = 0$, $m = 2$. The solution corresponding to the boundary segment BD in Fig. 4 describes a spatially periodic ensemble of cloud rolls (banks) separated by the distance $2L = 2\pi/\sqrt{R_{\mathrm{m}}|\lambda|}$ (Fig. 8). Each separate cloud roll consists of two circulation cells (the right and the left ones), and $x_0/L = (1 + |\lambda|^{-1})^{-1/2}$ within each of them. As $\lambda \to 0$, the ratio $x_0/L \to 0$, which means that a notable asymmetry exists in the distribution of sizes of regions with ascending and descending motions. Because there is no net mass flux within the cells, the intensity of rising motions by far exceeds the intensity of downward motions. Such distributions are frequently called 'peak' structures in the literature.

6.5 Domain of moist convective instability in the plane of defining parameters

We pass from the parameter plane (λ_0, λ) on which the solutions have already been obtained to the plane of the original parameters $(\tilde{E}^{-1} = E^{-1}/R_{\mathrm{m}},\ \tilde{R} = R/R_{\mathrm{m}})$. Expressing $E^{-1} \equiv \sqrt{T}$ and R in terms of λ_1^2 and λ_2^2 from (12) and

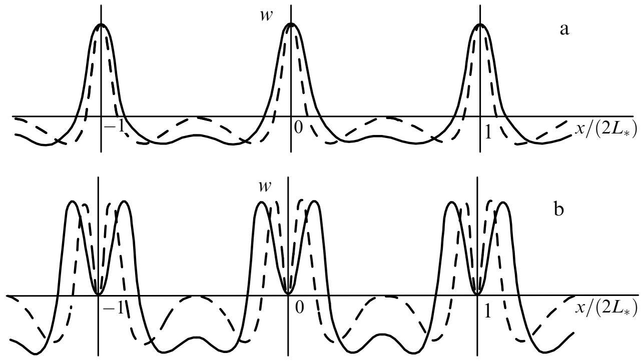

Figure 7. Spatial distributions of the vertical velocity $w(x)$ that correspond to the envelope of the first crests (solid curves) and second troughs (dashed curves) for (a) the first and (b) the second modes. The interval BD of the curve $\lambda = \psi(\lambda_0)$ in Fig. 4 is related to the distribution $w(x)$ shown by the solid line in panel a.

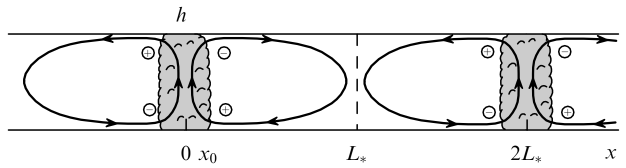

Figure 8. Schematics for streamlines of the first periodic mode that corresponds to the interval BD of the curve $\lambda = \psi(\lambda_0)$ in Fig. 4, in the xz plane. The '+' is for the velocity component v directed from the reader, and '$-$' for the one toward the reader.

normalizing by R_{m}, we find

$$\tilde{R} = 0.5(\lambda_0 + \lambda) - \sigma\,, \quad \tilde{E}^{-1} = 0.25\sqrt{(\lambda_0 - \lambda)^2 - 4\sigma^2}\,, \qquad (37)$$

where $\sigma = 2(1 + \kappa)/R_{\mathrm{m}}$. For given values of $\tilde{R}$ and $\tilde{E}^{-1}$, the fastest growth is exhibited by the solutions that correspond to the curve $\lambda = \psi(\lambda_0)$ in the plane (λ_0, λ). Indeed, for given $\tilde{R}$ and $\tilde{E}^{-1}$ and a fixed $\lambda < 1$, the magnitude of κ increases with λ_0. For solutions showing the fastest growths, the parameters λ_0 and λ are related by the dependence $\lambda = \psi(\lambda_0)$, and therefore relations (37) provide a parametric representation (with the parameter λ) of the curve $\sigma = \mathrm{const}$ in the plane $(\tilde{E}^{-1}, \tilde{R})$. When σ is fixed, drawing such a curve only requires using the part of the dependence $\lambda = \psi(\lambda_0)$ that satisfies the condition $-\infty < \lambda \leqslant \lambda_{\max}(\sigma)$, where $\lambda_{\max}(\sigma)$ is the root of the equation

$$\lambda_0 - \lambda = 2\sigma\,. \qquad (38)$$

For different values $\sigma \geqslant 0$, the curves in the plane $(\tilde{E}^{-1}, \tilde{R})$ fill the domain Ω shown in Fig. 9. In accordance with (37), $(\lambda = 0,\ \sigma = \sigma^* = 0.5\lambda_0^*)$ corresponds to the point $(\tilde{E}^{-1} = 0,\ \tilde{R} = 0)$, where $\lambda_0^* = 0.646$ is the root of the equation $f(\lambda_0) = 0$. Thus, the curve $\sigma^* = 0.323$ passes through the coordinate origin. Obviously, the instability region, i.e., the region where increasing solutions exist, is a part of the domain Ω bounded from above by the curve $\sigma = 2/R_{\mathrm{m}}$ $(\kappa = 0)$. The instability domain coincides with Ω in the limit $R_{\mathrm{m}} \to \infty$. For a fixed R_{m}, the curves $\sigma = \mathrm{const}$ are the isolines of the increment of most rapidly increasing perturbations, $\kappa = \sigma R_{\mathrm{m}}/2 - 1$.

The dashed lines in Fig. 9 correspond to the curves $\lambda = \mathrm{const}$; their equations can be easily derived in explicit

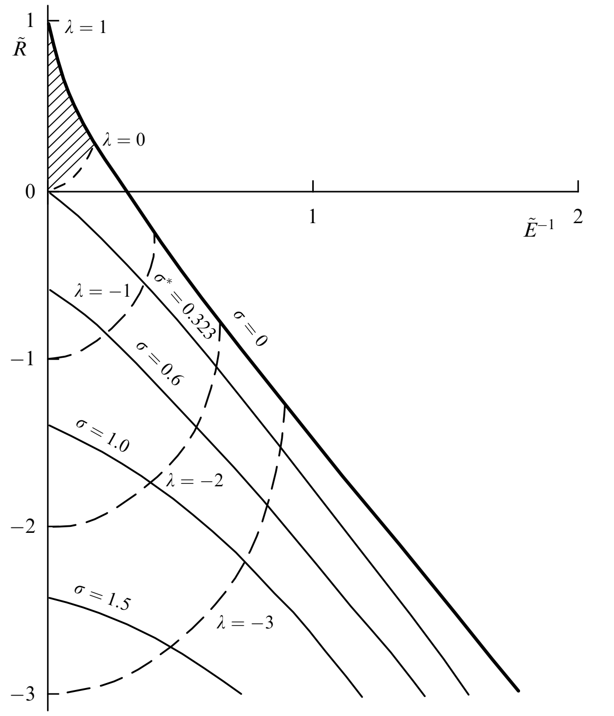

Figure 9. The domain Ω in the parameter plane $(\tilde{E}^{-1}, \tilde{R})$. The instability domain is bounded above by the curve $\sigma = 2/R_m$.

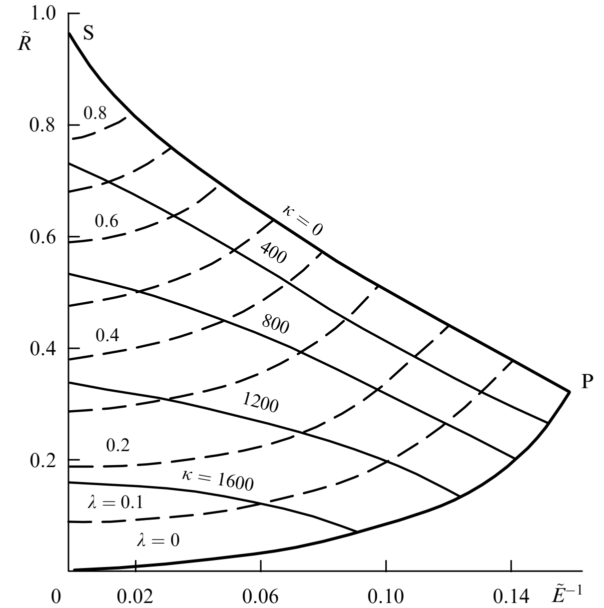

Figure 10. The subdomain of the instability domain where the first localized mode shows the fastest growth for $R_m = 1.2 \times 10^4$.

form by eliminating σ from relations (37). The curve $\lambda = 0$ passes through the origin and divides the domain Ω into two subdomains. For the point of intersection of the curves $\lambda = 0$ and $\sigma = 0$, we find $\tilde{E}^{-1} = 0.25\lambda_0^* \approx 0.16$ and $\tilde{R} = 0.5\lambda_0^* \approx 0.32$ from Eqn (37). The subdomain $0 \leqslant \lambda \leqslant 1$ is hatched. The instability domain contains a part of the hatched domain if the condition $\sigma \leqslant \sigma^*$ or $R_m \geqslant R_m^* = 2/\sigma^* \approx 6.19$ is satisfied. Within the hatched subdomain of the instability domain, the first localized mode has the fastest growth rate. As an example, the instability domain of the first localized mode is plotted separately in Fig. 10 for $R_m = 1.2 \times 10^4$. Instead of curves $\sigma = \text{const}$, the curves $\kappa = \text{const}$ are shown. For a fixed $R_m > R_m^*$, the curves $\lambda = \text{const}$ are such that the spatial structure of the localized mode does not change along them and is defined by relations (28), (34), and (35). In particular, the radius $x_0 = \pi/\sqrt{R_m(1-\lambda)}$ of the region with ascending motion of the localized mode does not change. In the subdomain of the instability domain considered here, the maximum value $\lambda_{\max}(\sigma)$ is attained by λ at the upper point S of the instability domain, which corresponds to $\sigma = 2/R_m$. From Eqn (38), for $R_m \gg 1$ we obtain the asymptotic expression $\lambda_{\max} \approx 1 - (\pi/R_m)^{2/3}$. Hence, inside the subdomain of the instability domain considered here, x_0 ranges from its minimum value $x_{0\,\min} = \pi/\sqrt{R_m}$ on the curve $\lambda = 0$ to its maximum value $x_{0\,\max} \approx \pi^{2/3}/R_m^{1/6}$ at the upper point of the instability domain. The corresponding dimensional values are obtained by multiplying by $\sqrt{\mu/\nu}\,h/\pi$. The instability increment reaches the maximum value $\kappa_{\max} = R_m/R_m^* - 1$ at the point of the instability domain that corresponds to the coordinate origin. The dimensional e-folding time is obtained by multiplying the quantity $1/\kappa_{\max}$ by the time scale $h^2/(\pi^2\nu)$.

In the lower subdomain of the instability domain, which embraces the entire instability domain for $R_m < R_m^* = 6.19$, the first periodic mode corresponding to the envelope of first crests is the most rapidly growing. For fixed R_m, the curves $\lambda = \text{const}$ are those on which the spatial structure of the periodic mode does not change, being defined by relations (33), (34), and (36). In particular, the quantities $x_0 = \pi/\sqrt{R_m(1+|\lambda|)}$, $L = \pi/\sqrt{R_m|\lambda|}$, and x_0/L stay constant. The transition from periodic solutions to localized ones on crossing the curve $\lambda = 0$ (the boundary between the subdomains) occur continuously.

The condition $R_m > R_m^* = 6.19$ is necessary and sufficient for the existence of the upper subdomain of the instability domain, where the localized perturbations realize the fastest growth rate. For $R_m < R_m^*$, only spatially periodic structures can be unstable.

For a fixed value of R_m, the upper boundary of the instability domain (the curve $\sigma = 2/R_m$) determines the dependence of the critical Rayleigh number on the Taylor (Ekman) number $R = R_{cr}(T)$. We find its limit form as $R_m \to 0$. To find the curve $\sigma = 2/R_m$, we take the fragment of the dependence $\lambda = \psi(\lambda_0)$ satisfying the condition $\lambda \leqslant \lambda_{\max}$. Because the curve $\lambda = \psi(\lambda_0)$ has the $\lambda \to -\infty$ asymptotic value $\lambda_0 = 1/2$, Eqn (32), it follows from Eqn (38) that $\lambda_{\max} = 1/2 - 4/R_m$. Hence, for the entire fragment of the curve $\lambda = \psi(\lambda_0)$, we have $|\lambda| \gg 1$ and $\lambda_0 \approx 1/2$. Eliminating λ from relations (37) and multiplying by R_m, we obtain the dependence $R = R_{cr}(T)$ in (9) for the dry Rayleigh convection. Simultaneously, we find $R_m|\lambda| = 4\sqrt{T+1}$ from Eqn (37), whence $L = \pi/(2(T+1)^{1/4})$. Taking the limit of the periodic solution in (33), (34), and (36) gives $w = \cos(\alpha x)$, $\alpha = \pi/(2L) = (1+T)^{1/4}$ up to a constant factor, which coincides with the most dangerous perturbation in Rayleigh model (9). Thus, for $R_m \to 0$ we observe a smooth transition from moist convection to the dry Rayleigh convection. The dependences $R = R_{cr}(T)$ for various values of R_m are shown in Fig. 11.

We write the main results in the case without rotation, $\tilde{E}^{-1} = 0$, which is of interest in and of itself. This case is associated with the upper point of the instability domain, for which Eqn (37) gives $\tilde{R}_{\max} = \lambda_{\max}$. With the asymptotic value

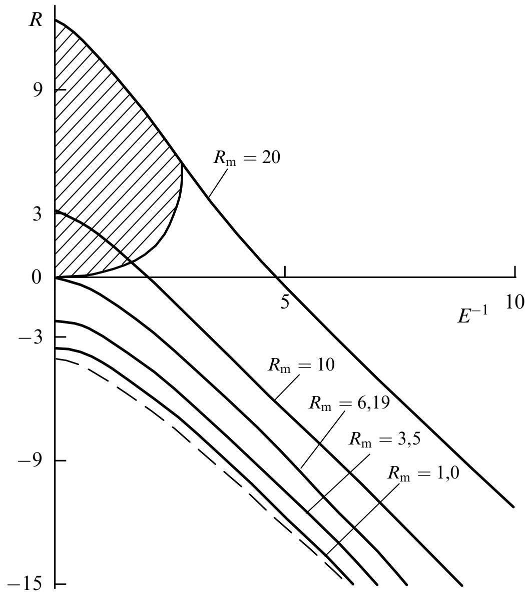

Figure 11. Boundaries of moist convective instability domains in the plane $E^{-1} \equiv \sqrt{T}$, R for various values of R_m. The dashed line is the respective curve for the dry Rayleigh convection ($R_m = 0$). Hatched is the subdomain of the instability domain for $R_m = 20$, where localized solutions demonstrate the fastest growth.

λ_{max} found above, we obtain the asymptotic form of the critical Rayleigh number R_{cr} in the absence of background rotation:

$$R_{cr} = -4 + \frac{R_m}{2}\,, \qquad R_m \ll 1;$$
$$R_{cr} \approx R_m\left(1 - \left(\frac{\pi}{R_m}\right)^{2/3}\right), \qquad R_m \gg 1\,. \tag{39}$$

For $R_m = R_m^*$, obviously, $R_{cr} = 0$. This relation, as well as the second relations in (39), can be rewritten in an alternative forms

$$\gamma_{cr} = \gamma_a\,, \quad R_m = R_m^*;$$
$$\gamma_{cr} = \gamma_m + (\gamma_a - \gamma_m)\left(\frac{\pi}{R_m}\right)^{2/3}, \quad R_m \gg 1\,. \tag{40}$$

We stress that for the upper subdomain of the instability domain, the value γ_{cr} always lies in the interval $\gamma_m < \gamma_{cr} \leqslant \gamma_a$, which corresponds to the conditionally unstable stratification. Neutral solutions corresponding to R_{cr} are localized for $R_{cr} \geqslant 0$ ($R_m \geqslant R_m^*$) and are periodic for $R_{cr} < 0$. For neutral solutions, Eqns (28) and (33) lead to $x_0 = \pi/\sqrt{R_m - R_{cr}}$ and $L = \pi/\sqrt{|R_{cr}|}$, where second relation pertains to only periodic solutions. For localized neutral solutions, we have the asymptotic formula $x_0 \approx \pi^{2/3}/R_m^{1/6}$, $R_m \gg 1$. For $R_m = R_m^*$, we have $x_0 = \pi/\sqrt{R_m^*}$. For periodic neutral solutions, we obtain the asymptotic formulas $x_0 \approx (1 - R_m/16)\pi/2$ and $L \approx (1 + R_m/16)\pi/2$, $R_m \ll 1$. As can be seen, already for $R_m \ll 1$, taking phase transitions in the Rayleigh model into account deforms the symmetric dry convective cell such that the region of downward motions becomes wider than the region of rising motions, while the cell size $L_* = x_0 + L$ remains the same in the first approximation.

The instability domain of the second mode is structured similarly. It lies within the instability domain of the first mode and is qualitatively similar. For the second mode, the corresponding value is $R_m^* = 8.75$, and the mode always unfolds more slowly than the first mode.

We note that the radius L of the region of descending motions for the most unstable first periodic mode coincides with that for the oscillating Green's function G: $L = L_G = \pi/\sqrt{R_m|\lambda|}$. This underlies the mechanism whereby the spatial structure of the oscillating Green's function influences the structure of the most unstable spatially periodic solution.

We briefly summarize this section. Taking phase transitions of moisture into account leads to principle distinctions between the moist convection and the dry Rayleigh convection. In the parameter plane, the region of moist convective instability generally consists of two subdomains, in one of which the fastest growth is exhibited by localized convective rolls, and in the second by spatially periodic systems of convective rolls with narrow (concentrated) regions of rising motions.

7. Localized axisymmetric structures (convective vortices)

In this section, we construct localized axisymmetric solutions of integral equation (15) — analogs of the localized convective rolls considered in Section 6. These solutions describe convective vortices with various spatial scales, in the range from a single cloud to a tropical cyclone.

For axisymmetric perturbations $w = w(r)$ satisfying the condition of sign definiteness $w(r) \geqslant 0$, $r \in (0, r_0)$; $w(r) \leqslant 0$, $r > r_0$, Eqn (15) reduces to the equation

$$w(r) = R_m \int_0^{r_0} G(\rho, r)\, w(\rho) \rho\, d\rho\,, \tag{41}$$

$$G(\rho, r) = \frac{1}{\lambda_1^2 - \lambda_2^2} \times \begin{cases} \lambda_1^2 K_0(\lambda_1 r)\, I_0(\lambda_1 \rho) - \lambda_2^2 K_0(\lambda_2 r)\, I_0(\lambda_2 \rho)\,, & \rho < r\,, \\ \lambda_1^2 K_0(\lambda_1 \rho)\, I_0(\lambda_1 r) - \lambda_2^2 K_0(\lambda_2 \rho)\, I_0(\lambda_2 r)\,, & \rho > r\,, \end{cases}$$

with the obvious boundary condition $w(r_0) = 0$. Here, $I_n(r)$ and $K_n(r)$ are the modified Bessel functions. The eigenvalues $\lambda_{1,2}^2$ defined by formula (12) are considered real-valued and positive in what follows.

Solutions of Eqn (41) are sought in a form analogous to Eqn (19):

$$w(r) = \frac{J_0(p_1 r)}{J_0(p_1 r_0)} - \frac{J_0(p_2 r)}{J_0(p_2 r_0)}\,, \qquad 0 < r < r_0\,, \tag{42}$$

where $J_n(r)$ is the Bessel function. Substituting Eqn (42) in Eqn (41) and equating the coefficients at $J_0(p_j r)$ in the left- and right-hand sides, we arrive, as previously, at expressions (20) for the parameters $p_2 > p_1$. The requirement that the coefficient at $I_0(\lambda_j r)$ in the right-hand side be zero leads to two equations, which after simple rearrangement can be written as

$$\frac{J_1(p_j r_0)}{J_0(p_j r_0)} = A_j \frac{K_1(\lambda_1 r_0)}{K_0(\lambda_1 r_0)} - B_j \frac{K_1(\lambda_2 r_0)}{K_0(\lambda_2 r_0)}\,, \qquad j = 1, 2\,, \tag{43}$$

where

$$A_j = \frac{\lambda_2 (p_j^2 + \lambda_1^2)}{p_j (\lambda_1^2 - \lambda_2^2)}\,, \qquad B_j = \frac{\lambda_1 (p_j^2 + \lambda_2^2)}{p_j (\lambda_1^2 - \lambda_2^2)}\,.$$

Because p_j and λ_j can be expressed in terms of λ_0 and λ using relations (20), Eqns (43) form a system that connects the three parameters λ_0, λ, and $Z_0 = 0.5R_\mathrm{m}r_0$. Eliminating the parameter Z_0 from Eqns (43) formally leads to a functional dependence $\lambda = f(\lambda_0)$. As for plain localized modes, this dependence furnishes the existence of a nontrivial solution and is used in analyzing the instability domain.

We can derive the asymptotic form of the dependence $\lambda = f(\lambda_0)$ assuming that $p_j r_0, \lambda_j r_0 \gg 1$. Using the asymptotic representation for the Bessel function, we find the equations $\tan(p_{1,2}r_0 - \pi/4) = \pm(\lambda_0^{-1} - 1)^{1/2}$ from Eqns (43); hence,

$$
\begin{aligned}
p_1 r_0 - \frac{\pi}{4} &= \arctan\sqrt{\lambda_0^{-1} - 1} + \pi n\,, \\
p_2 r_0 - \frac{\pi}{4} &= -\arctan\sqrt{\lambda_0^{-1} - 1} + \pi m\,,
\end{aligned}
\tag{44}
$$

where $n \geqslant 0$, $m > n$. Adding Eqns (44) gives

$$
r_0 = \frac{\pi(n + m + 1/2)}{\sqrt{R_\mathrm{m}(1 - \lambda)}}\,. \tag{45}
$$

Eliminating the parameter r_0 from Eqns (44) leads to the functional dependence

$$
\begin{aligned}
\lambda = f(\lambda_0) &= 1 - (1 - \lambda_0) \\
&\times \left(\frac{m - n}{n + m + 1/2} - \frac{2}{\pi(n + m + 1/2)} \arcsin\sqrt{1 - \lambda_0} \right)^{-2},
\end{aligned}
\tag{46}
$$

which breaks into a set of branches and is analogous to dependence (29) for plane localized modes.

To accurately find the branches of the dependence $\lambda = f(\lambda_0)$, a suitable numerical algorithm was proposed in Ref. [22]. Setting $x_1 = p_1 r_0$ and $x_2 = p_2 r_0$ and using relation (20), we rewrite system (43) in the form

$$
J_1(x_j) = F_j(x_j, \lambda_0, \lambda) J_0(x_j)\,, \quad j = 1, 2; \quad \frac{x_1}{x_2} = \frac{p_1(\lambda_0, \lambda)}{p_2(\lambda_0, \lambda)}\,, \tag{47}
$$

where the expressions for F_j directly follow from Eqns (43). For given λ_0 and λ, each of the first two equations has a countable set of roots, x_1^n, x_2^n, $n = 1, 2, \ldots$, enumerated in ascending order. It can be shown that $x_1^n \in (\mu_{n-1}^{(1)}, \mu_n^{(0)})$ and $x_2^n \in (\mu_{n-1}^{(0)}, \mu_n^{(0)})$, where $\mu_i^{(0)}$ and $\mu_i^{(1)}$ are zeros of the Bessel functions of the zeroth and first order for $i \neq 0$, $\mu_0^{(0)} = \mu_0^{(1)} = 0$. For a fixed $\lambda \in (0, 1)$, for every $1 > \lambda_0 > \lambda$, the roots $x_1 = x_1^n$ from the interval with the number n and $x_2 = x_2^m$ from the interval with a number $m > n$ have been determined, which corresponds to selecting a certain branch of the dependence $\lambda = f(\lambda_0)$. The value of λ_0 for which $x_1/p_1 = x_2/p_2$, together with the value of λ, defines the branch of the dependence. Simultaneously, the value of $r_0 = x_1/p_1$ is also automatically determined. Expressions (45) and (46) give the asymptotic form of r_0 and of the branches as $\lambda \to 0$.

Examination of the sign definiteness of the solution is carried out by resorting to the explicit expression for the solution

$$
w(r) = \begin{cases} \dfrac{J_0(p_1 r)}{J_0(p_1 r_0)} - \dfrac{J_0(p_2 r)}{J_0(p_2 r_0)}\,, & 0 < r < r_0\,, \\[2ex] \dfrac{p_2^2 - p_1^2}{\lambda_1^2 - \lambda_2^2} \left(\dfrac{K_0(p_1 r)}{K_0(p_1 r_0)} - \dfrac{K_0(p_2 r)}{K_0(p_2 r_0)} \right), & r > r_0\,, \end{cases}
$$

and the information obtained on the localization of roots $x_{1,2} = p_{1,2} r_0$. The analysis shows that the condition $w(r) \geqslant 0$, $r \in (0, r_0)$ is only satisfied for $p_1 r_0 \in (0, \mu_1^{(0)})$, $p_2 r_0 \in (\mu_1^{(0)}, \mu_2^{(0)})$. Hence, in contrast to the two-dimensional problem with planar geometry, there is only a single localized symmetric mode that satisfies the conditions formulated above. It is characterized by $n = 0$, $m = 1$ in asymptotic relations (44)–(46). A given $w(r)$ distribution for this mode uniquely defines the distributions of radial $u(r)$ and tangential $v(r)$ velocity components, and, as previously, the tangential velocity component occurs only because of the torsion action of the Coriolis force. The mode obtained describes a convective vortex with a structure characteristic of tropical cyclones at their earlier development stage [6]: there is a cyclonic circulation with mass inflow onto the axis of the vortex in the lower half of the layer replaced by an anticyclonic circulation and outflow in its upper half.

The curve $\lambda = f(\lambda_0)$ for the axisymmetric localized mode in the plane (λ_0, λ) everywhere except the point $\lambda_0 = \lambda = 1$ lies to the right of the curve $\lambda = f(\lambda_0)$ for the first plane localized mode. Therefore, for fixed problem parameters, the fastest growth is attained by the localized axisymmetric mode. Its instability region can also be found using the dependence $\lambda = f(\lambda_0)$ and relations (37), which define a map to the plane of normalized parameters $(\tilde{E}^{-1}, \tilde{R})$. This region only exists for $R_\mathrm{m} > 5.04$ and is qualitatively similar to that of the first localized plane mode (see Fig. 10) that lies everywhere inside the instability region of the localized axisymmetric mode. For the axisymmetric mode, the curves $\lambda = \mathrm{const}$ are those along which the mode spatial structure does not vary; in particular, the radius r_0 of the region of ascending motions remains the same. The maximum value of r_0 is reached at the upper point of the instability region; for $R_\mathrm{m} \gg 1$, the radius is $r_{0\max} \approx (2\mu_1^{(1)})^{1/2}(\ln R_\mathrm{m})^{-1/4}$. The minimum value of r_0 corresponds to the curve $\lambda = 0$; from Eqn (49), taking $n = 0$, $m = 1$, we have $r_{0\min} \approx 3\pi/(2\sqrt{R_\mathrm{m}})$.

In general, the instability region in the parameter plane $(\tilde{E}^{-1}, \tilde{R})$ should be continued below the curve $\lambda = 0$ for the axisymmetric localized mode. Apparently, in the lower subdomain of the instability region (for $R_\mathrm{m} > 5.04$), the maximum growth rate is shown by cell structures whose spatial period tends to infinity as the boundary between the subdomains $\lambda = 0$ is approached and the radius of the ascending motion region inside the cell tends to $r_{0\min}$.

8. Numerical estimates for localized modes

For $R_\mathrm{m} \gg R_\mathrm{m}^*$, the dimensionless radii of the region of ascending motion for localized modes, $x_{0\max}$ and $r_{0\max}$, depend on R_m very weakly, and the corresponding dimensional value is largely determined by the combination $h\sqrt{\mu/\nu}$. We take a set of parameters characteristic of the troposphere to make estimates [3, 4]: $f \approx 10^{-4}$ s^{-1}, $\alpha \approx 3 \times 10^{-3}$ K^{-1}, $\gamma_\mathrm{a} \approx 10^{-2}$ K m^{-1}, and $\gamma_\mathrm{m} \approx 6.4 \times 10^{-3}$ K m^{-1}. In numerical models of large-scale motions (with a size comparable to that of a tropical cyclone), it is commonly assumed [6] that $h \approx 10^4$ m, $\mu \approx 10^5$ m^2 s^{-1}, and $\nu \approx 10$ m^2 s^{-1}. In this case, $R_\mathrm{m} \approx 1.2 \times 10^4$ and $\tilde{E}^{-1} \approx 10^{-2}$, which practically corresponds to the absence of background rotation, $R_\mathrm{cr} \approx R_\mathrm{m}$ and $\gamma_\mathrm{cr} \approx \gamma_\mathrm{m}$. In dimensional form, we have $x_{0\min} \approx 10$ km, $x_{0\max} \approx 140$ km, $r_{0\min} \approx 15$ km, and $r_{0\max} \approx 300$ km. The selected value for the horizontal viscosity μ corresponds to motions with the scale $x_{0\max}$, $r_{0\max}$. Therefore, for the parameter values specified above, a localized axisymmetric vortex exponentially growing with time has the structure and size of a tropical cyclone at its early development stage, while a localized convective roll can be regarded as its plane analog. For motions with the scale $x_{0\,\min}$, $r_{0\,\min}$, the selected value of μ is excessively high. We consider motions with the size of an isolated cloud $h \approx 10^3$ m and $\mu \approx 10^2$ m^2 s^{-1}, and keep the other parameters unchanged. We then have $R_{\mathrm{m}} \approx 1.2 \times 10^3$ and $\tilde{E}^{-1} \approx 10^{-3}$, and in the dimensional form, $x_{0\,\min} \approx 100$ m, $x_{0\,\max} \approx 700$ m, $r_{0\,\min} \approx 150$ m, and $r_{0\,\max} \approx 1.5$ km, which correspond to the horizontal scales of convective clouds by an order of magnitude.

9. Some experimental data and results of numerical simulations

The solutions obtained above describe only the initial stage of instability development, because we dropped the nonlinear advective terms in the system of dynamical equations. Numerical simulations of moist convection with the full equations have been performed in numerous papers [7–15]; the simulations consisted in separate numerical experiments. A comparison with numerical results indicates that the main features of analytic solutions carry over to the full nonlinear models.

As a demonstrative example, we mention Ref. [12], which dealt with the full two-dimensional system of equations of thermal convection with a latent heat source of condensation taken into account in form (5). The spectral method was used to work out the system, with periodic boundary conditions at the horizontal boundaries of the computational domain. Varying the stratification parameter γ, the author of Ref. [12] studied the process of the onset and equilibration of moist convection in a layer of the atmosphere with the thickness $h = 1$ km, triggered by a random temperature perturbation at the initial instant. Figure 12 displays horizontal distributions of the vertical velocity obtained in Ref. [12] for successive instants for $\gamma - \gamma_{\mathrm{a}} = 3 \times 10^{-3}$ K m^{-1}. It is clearly seen how narrow regions of intense rising motions are formed as the convection process is unfolding, being separated by broad regions of downward motions of practically zero velocity. With the advective terms taken into account, the convective 'peak' structures evolve into a stationary regime, the equilibration time being from two to ten hours. Some distinctions in peak heights in Fig. 12 are most probably of numerical origin.

A physically more rigorous model of moist convection has been considered in Ref. [14]. This model dealt with a rather complex structure of the convective boundary layer comprising a thin surface layer with constant fluxes, a layer of free convection, and a cloud layer proper with unstable stratification. The latent heat source in the model in Ref. [14] was 'switched on' only when the ascending air reached the level of condensation (it stayed equal to zero for downward motions). The results of one simulation from Ref. [14] are presented in Fig. 13. It can be seen that in these simulations, periodic cloud structures (cloud banks) also form with narrow concentrated regions of ascending motions.

We briefly discuss some results of meteorological observations. The processes of moist convection are most prominent in the boundary layer over the surface of oceans and seas, in particular, during so-called cold outbreaks — outflows of cold polar air over the surface of warm Nordic seas. Satellite images of this area show various ordered structures in the form of periodic cloud rolls: open or closed spatial convective cells (respectively with ascending or descending convective motions at the cell center). It was long ago that the

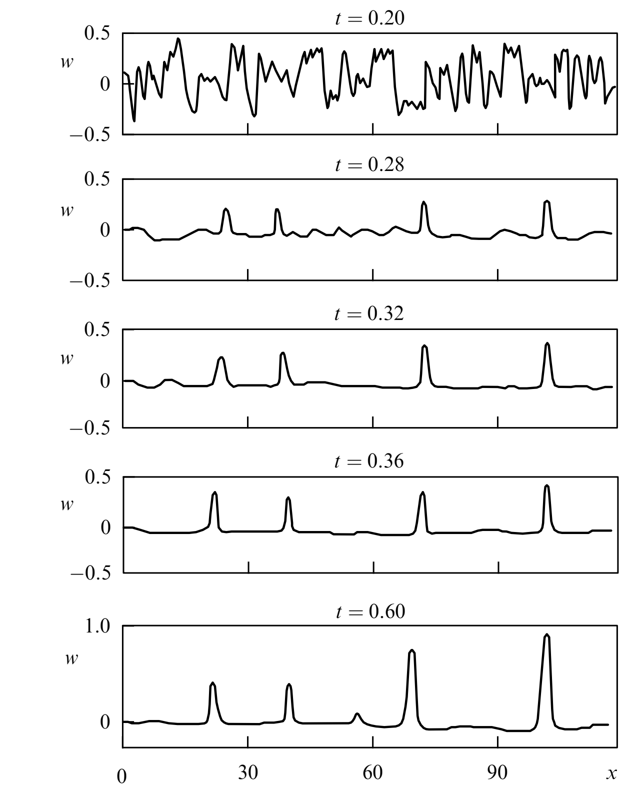

Figure 12. Horizontal profiles of the vertical velocity at successive instants of time, obtained in Ref. [12].

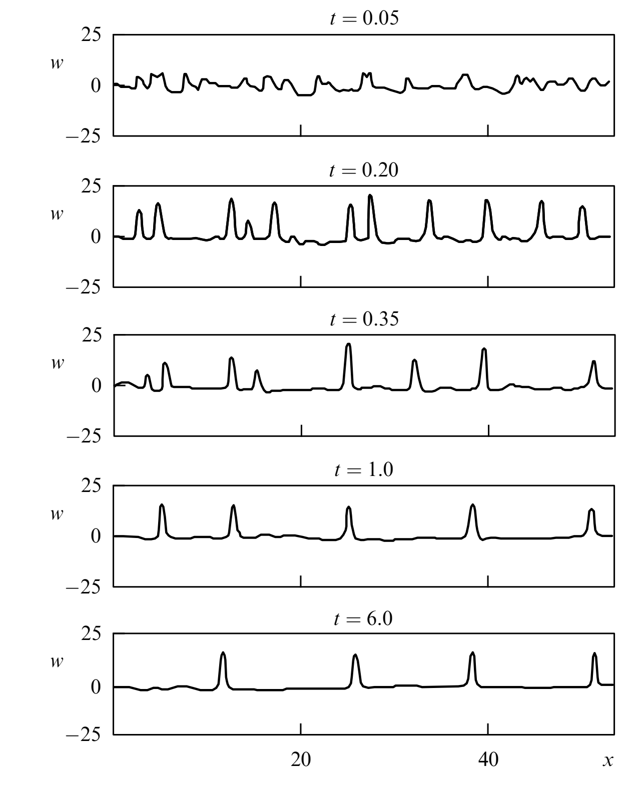

Figure 13. Horizontal profiles of the vertical velocity at successive instants of time, obtained in Ref. [14].

discrepancy between the observed parameters of cloud structures and the Rayleigh model predictions was established. The first discrepancy concerns the aspect ratio of a convective cell, i.e., the ratio of its horizontal size to the vertical one. While this ratio is 2 to 3 in the Rayleigh model (depending on the form of the boundary conditions), it can be an order of magnitude larger for the observed cloud structures [11, 12, 27]. The other apparent discrepancy is related to the observed asymmetry between ascending and descending motions: the area covered by clouds or the area of ascending motion can make up less than 10% of the entire area involved in ordered convection [12, 27]. As shown above, at least at a qualitative level, these discrepancies are explained by the impact of phase transitions involving moisture in convection.

10. Conclusions (brief summary)

Convective motions in moist saturated air are accompanied by the release of latent condensation heat. Taking this effect into account, we considered the problem of convective instability in a layer of moist saturated air, which generalizes the classic Rayleigh problem. We presented an analytic solution of the problem that demonstrates the principal differences between moist convection and Rayleigh convection. In general, the instability domain in the plane of control parameters consists of two subdomains; in one of them, the fastest growth rate is realized for localized convective rolls (planar geometry of the problem) or localized axisymmetric vortices with the structure of a tropical cyclone at its early development phase. Depending on the parameter values, their spatial scale ranges from the scale of an isolated cloud to that of tropical cyclones. We have found a necessary and sufficient condition for the existence of this subdomain. In the second subdomain, the fastest growth is realized for nonlinear structures that are periodic in space, their spatial period tending to infinity on the boundary between the subdomains. They are characterized by essential localization of the regions of ascending motions within each convective cell, such that the fraction of the atmosphere area covered by clouds is strictly less than unity and tends to zero as the boundary between the subdomains is approached. We demonstrated the transition to Rayleigh convection in the hydrostatic approximation.

11. Conclusions (future tasks)

We mention some questions still awaiting further theoretical analysis. In the framework of the model discussed here, they include the question of the spatial structure of three-dimensional convective cells of the fastest growth, and the question of stability of the solutions found. A more accurate description of the formation of small-scale cloud structures can only be obtained with a model that does not resort to the hydrostatic approximation. In the absence of background rotation, such a model was recently developed in Ref. [28]. Just as for the Rayleigh convection, exploring supercritical nonlinear regimes of convection based on the corresponding amplitude equations is of principal importance.

The authors thank E A Kuznetsov for the interest in this work and the invitation to present the results at the annual session of the Nonlinear Dynamics Council of RAS.

References

1. Landau L D, Lifshitz E M *Fluid Mechanics* (Oxford: Pergamon Press, 1987) [Translated from Russian: *Gidrodinamika* (Moscow: Nauka, 1986)]
2. Gershuni G Z, Zhukhovitskii E M *Konvektivnaya Ustoichivost' Neszhimaemoi Zhidkosti* (Convective Stability in Incompressible Fluids) (Moscow: Nauka, 1972)
3. Gill A E *Atmosphere-Ocean Dynamics* (New York: Academic Press, 1982) [Translated into Russian (Moscow: Mir, 1986)]
4. Matveev L T *Kurs Obshchei Meteorologii. Fizika Atmosfery* (A Course of General Meteorology. Atmospheric Physics) (Leningrad: Gidrometeoizdat, 1984)
5. Emanuel K A *Atmospheric Convection* (New York: Oxford Univ. Press, 1994)
6. Khain A P *Matematicheskoe Modelirovanie Tropicheskikh Tsiklonov* (Mathematical Modeling of Tropical Cyclones) (Leningrad: Gidrometeoizdat, 1989)
7. Asai T, Nakasuji I *J. Meteorolog. Soc. Jpn. II* **60** 425 (1982)
8. Asai T, Nakasuji I *J. Meteorolog. Soc. Jpn. II* **55** 151 (1977)
9. Bretherton C S *J. Atm. Sci.* **44** 1809 (1987)
10. Yamasaki M *J. Meteorolog. Soc. Jpn. II* **52** 365 (1974)
11. Yamasaki M *J. Meteorolog. Soc. Jpn. II* **50** 465 (1972)
12. van Delden A *Beitr. Phys. Atmos.* **58** 202 (1985)
13. Huanq X-Y *Tellus A* **42** 270 (1990)
14. Chlond A *Beitr. Phys. Atmos.* **61** 312 (1988)
15. Huang X-Y, Källén E *Tellus A* **38** 381 (1986)
16. Haque S M *Quart. J. R. Meteorolog. Soc.* **78** 394 (1958)
17. Kuo H L *Tellus* **13** 441 (1961)
18. Lilly D K *Mon. Weather Rev.* **88** 1 (1960)
19. Gill A, in *Intense Atmospheric Vortices* (Eds L Bengtsson, J Lighthill) (Berlin: Springer-Verlag, 1982) [Translated into Russian (Moscow: Mir, 1985) p. 130]
20. Shmerlin B Ya, Kalashnik M V *Izv. Atmos. Ocean. Phys.* **25** 307 (1989) [*Izv. Akad. Nauk SSSR Fiz. Atmos. Okeana* **25** 421 (1989)]
21. Shmerlin B Ya, Kalashnik M V *Izv. Atmos. Ocean. Phys.* **25** 599 (1989) [*Izv. Akad. Nauk SSSR Fiz. Atmos. Okeana* **25** 810 (1989)]
22. Kalashnik M V, Shmerlin B Ya *Izv. Atmos. Ocean. Phys.* **26** 577 (1990) [*Izv. Akad. Nauk SSSR Fiz. Atmos. Okeana* **26** 787 (1990)]
23. Kalashnik M V, Shmerlin B Ya *Izv. Atmos. Ocean. Phys.* **26** 759 (1990) [*Izv. Akad. Nauk SSSR Fiz. Atmos. Okeana* **26** 1034 (1990)]
24. Gutman L N *Vvedenie v Nelineinuyu Teoriyu Mezometeorologicheskikh Protsessov* (Introduction into the Nonlinear Theory of Mesoscale Meteorological Processes) (Leningrad: Gidrometeoizdat, 1969)
25. Belov P N *Prakticheskie Metody Chislennogo Prognoza Pogody* (Practical Methods for Numerical Weather Forecast) (Leningrad: Gidrometeoizdat, 1967)
26. Kalashnik M V, Ingel L Kh *Izv. Akad. Nauk SSSR Fiz. Atmos. Okeana* **24** 1327 (1988)
27. Agee E A *Dyn. Atmos. Oceans* **10** 317 (1987)
28. Shmerlin B Ya, Kalashnik M V, Shmerlin M B *JETP* **115** 1111 (2012) [*Zh. Eksp. Teor. Fiz.* **142** 1265 (2012)]